Supplemental Figures

Fig. S1. Multiple sequence alignments for C-terminal domains of NS1 molecules from influenza A and B viruses.

Fig. S2. Backbone chemical shift perturbations of NS1B CTD due to dsRNA binding, mapped along the protein sequence.

Fig. S3. [^{15}N-^{1}H]-HSQC spectra of surface Lys or Arg to Ala mutants demonstrate that these mutants maintain a native 3D structure.

Fig. S4. Analytical gel filtration with multi-angle static light scattering detection (AGF-MALS) for wt NS1B CTD.

Fig. S5. Analytical ultracentrifugation analysis of NS1B CTD.

Fig. S6 Concentration dependence of ^{15}N-^{1}H backbone chemical shifts for NS1B CTD.

Fig. S7. The NS1A CTD from influenza A virus does not bind dsRNA.

Fig. S8. NMR triple-resonance connectivity maps for backbone resonance assignments of wild-type and [R238A]-NS1B CTD.

Figure S1. Related to Figures 1 and 7. Multiple sequence alignments for C-terminal domains (CTDs) of NS1 molecules from influenza A and B viruses. (a) NS1A CTD sequences from influenza A viruses. (b) NS1B CTD sequences from influenza B viruses. The locations of basic residues in the NS1B CTD (panel b) contributing to RNA binding activity are indicated by green circles.

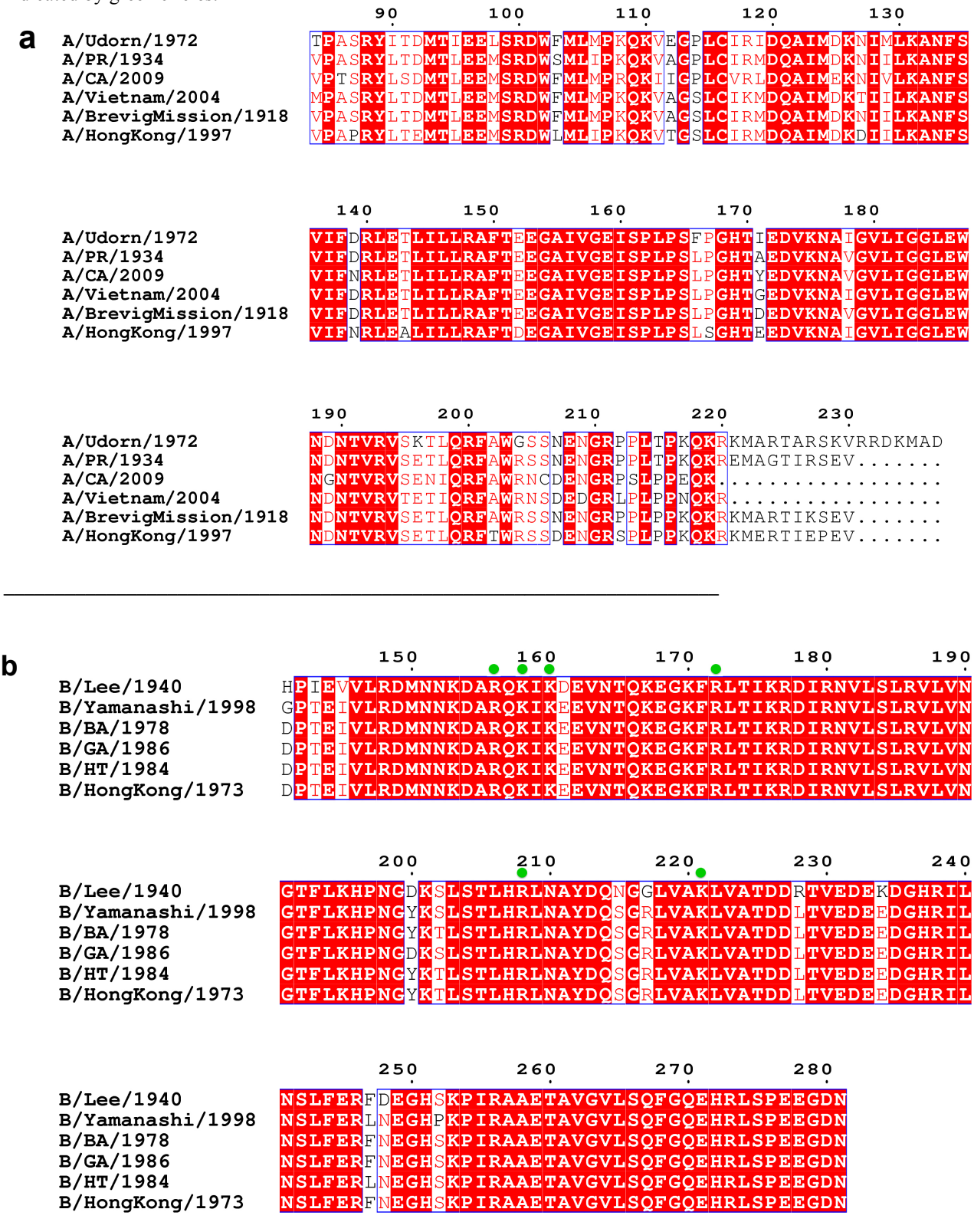

Figure S2. Related to Figure 1d. Backbone chemical shift perturbations of NS1B CTD due to dsRNA binding, mapped along the protein sequence. Composite chemical shift changes $\Delta\delta_{comp}$ due to dsRNA binding were measured by [^{15}N-^{1}H]-HSQC NMR experiments, as described in the Methods section. The threshold for defining a significant chemical shift perturbation (CSP) was determined from the following iterative analysis. The standard deviation (σ) of the shift changes was first calculated. To prevent biasing the distribution by including the small number of residues with very large shift changes, any residues for which the shift change is greater than 3σ were excluded. The next standard deviation was then recalculated excluding residues with shift changes more than 3σ. Iteration of these calculations was performed until no further residues are excluded, resulting in deviation for unperturbed sites of $3\sigma = 0.018$ ppm. Accordingly, we choose 0.02 ppm (20 ppb) as the threshold to minimize any false positives. The solid horizontal line is drawn at 20 ppb, and the dashed horizontal line at 30 ppb, corresponding to cutoffs used for light blue ($20 < \Delta\delta_{comp} < 30$ ppb), and dark blue ($\Delta\delta_{comp} \geq 30$ ppb) highlighting, respectively, in Figure. 1d.

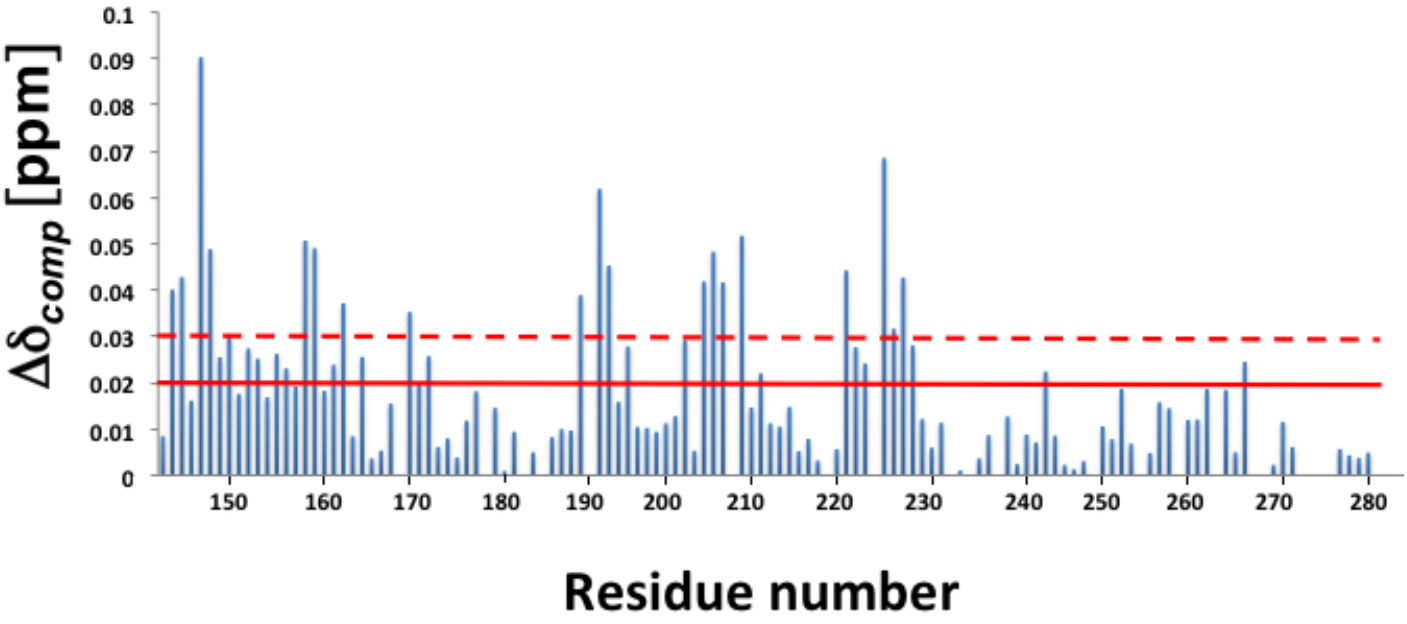

Figure S3. Related to Figure 2. **[^{15}N-^{1}H]-HSQC spectra of surface Lys or Arg to Ala mutants demonstrate that these mutant proteins maintain a native 3D structure.** Overlays of 600 MHz [^{15}N-^{1}H]-HSQC spectra of wt NS1B CTD, blue, and 9 Lys or Arg to Ala mutants, red. Spectra were recorded using protein concentrations of 0.1 to 0.2 mM CTD variants, at pH 5.5, and temperature of 298 K.

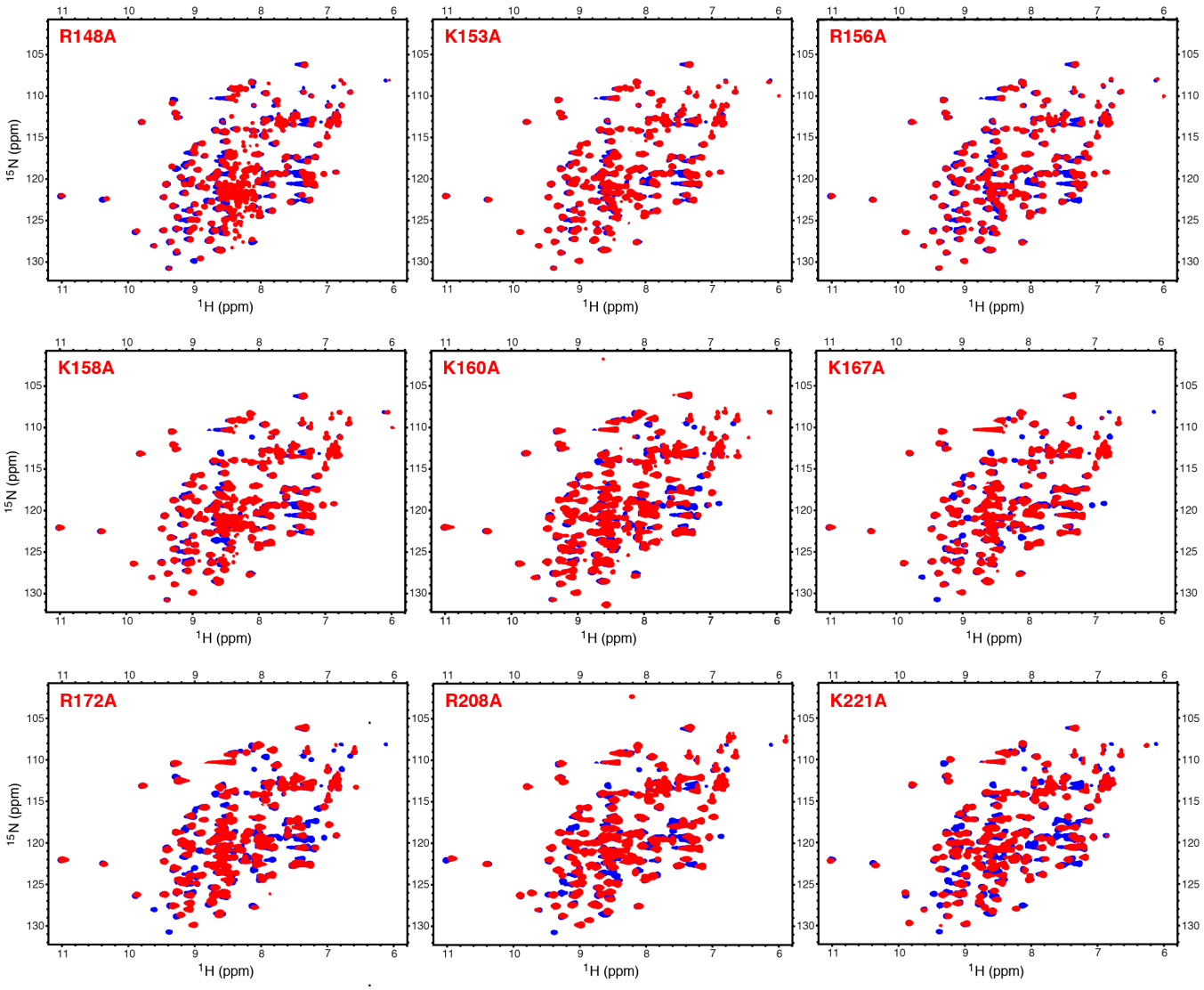

Figure S4. Related to Figure 3. Analytical gel filtration with multiangle static light scattering detection (AGF-MALS) for wt NS1B-CTD. Using an initial protein concentration of ~ 200 μM, AFG-MALS demonstrates a monodisperse monomer. The protein sample (30 μl) was injected onto an analytical gel-filtration column (Shodex KW-802.5, Showa Denko, Japan) with the effluent monitored by refractive index (black trace, Optilab rEX) and 90° static light-scattering amplitude (blue trace; miniDAWN TREOS, Wyatt Technology) detectors. The resulting experimental molecular weight is 17.0 kDa (red), with is in good agreement with the expected MW of 15.9 kDa for a monomeric species.

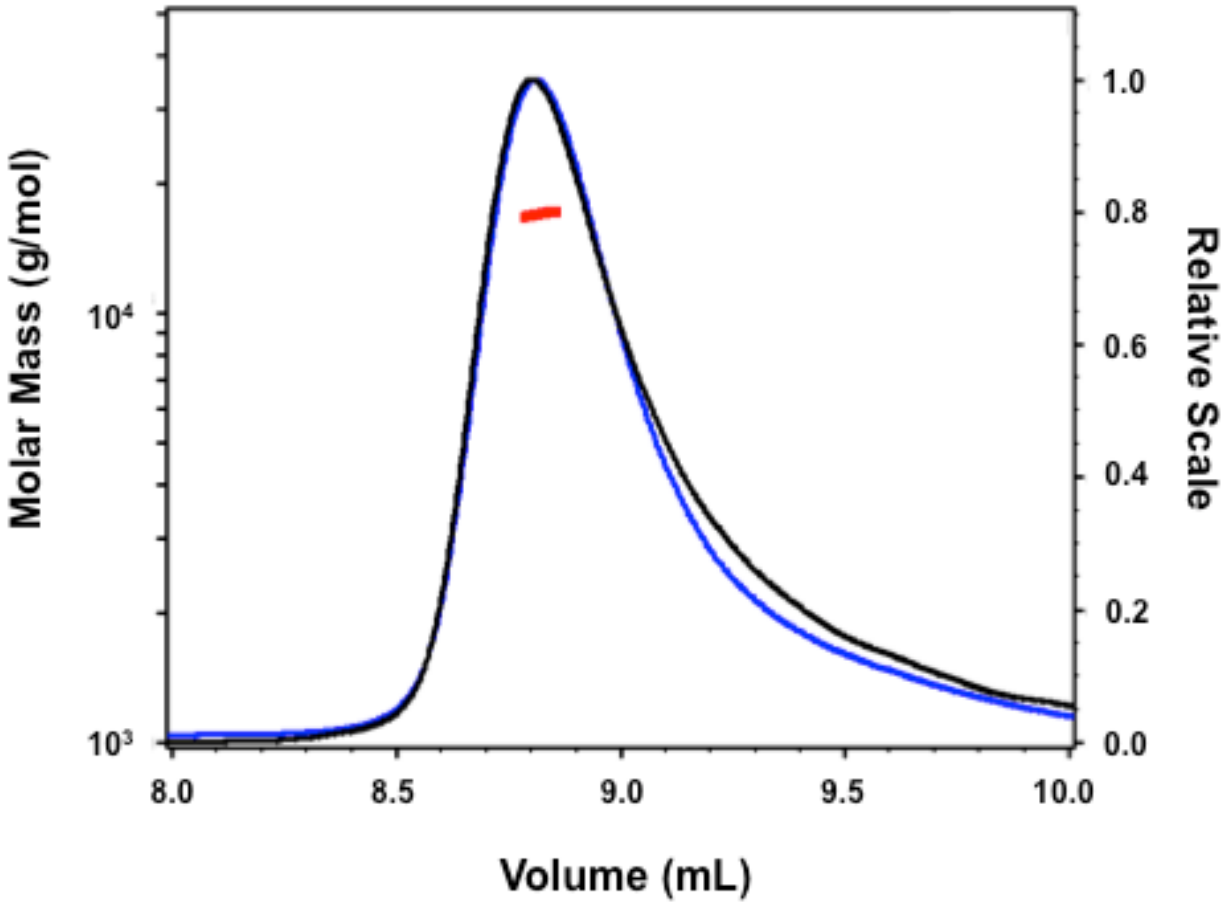

Figure S5. Related to Figure 3. Analytical ultracentrifugation (AUC) analysis of NS1B CTD. AUC measurements were carried out on samples with initial concentrations ranging from 13 to 100 μM. In all of these runs, AUC detected a homogeneous single peak corresponding to monomeric NS1B CTD (MW 15.2 ± 0.3 kDa), with only small amounts of faster sedimenting aggregate(s). Over the concentration range covered by these protein samples, no significant amounts of dimer or higher order oligomers in equilibrium with the predominant monomeric species were detected, indicating a K_d for dimerization > ~ 200 μM. Protein samples were prepared in 20 mM NH_4OAc, 450 mM NaCl, 5 mM $CaCl_2$, 50 mM arginine, 0.02% NaN_3, at pH 5.5, the same buffer used for the NMR structural studies. Normalized sedimentation coefficient distributions c(s) are shown for runs made with NS1B CTD at initial protein concentrations of 13 μM (red trace), 26 μM (green trace), 47 μM (blue trace) and 94 μM (black trace). The c(s) distributions have been normalized for the different protein concentrations used. There was no indication of dimerization over the range of concentrations studied, although a small amount of irreversible aggregation was observed at higher protein concentrations.

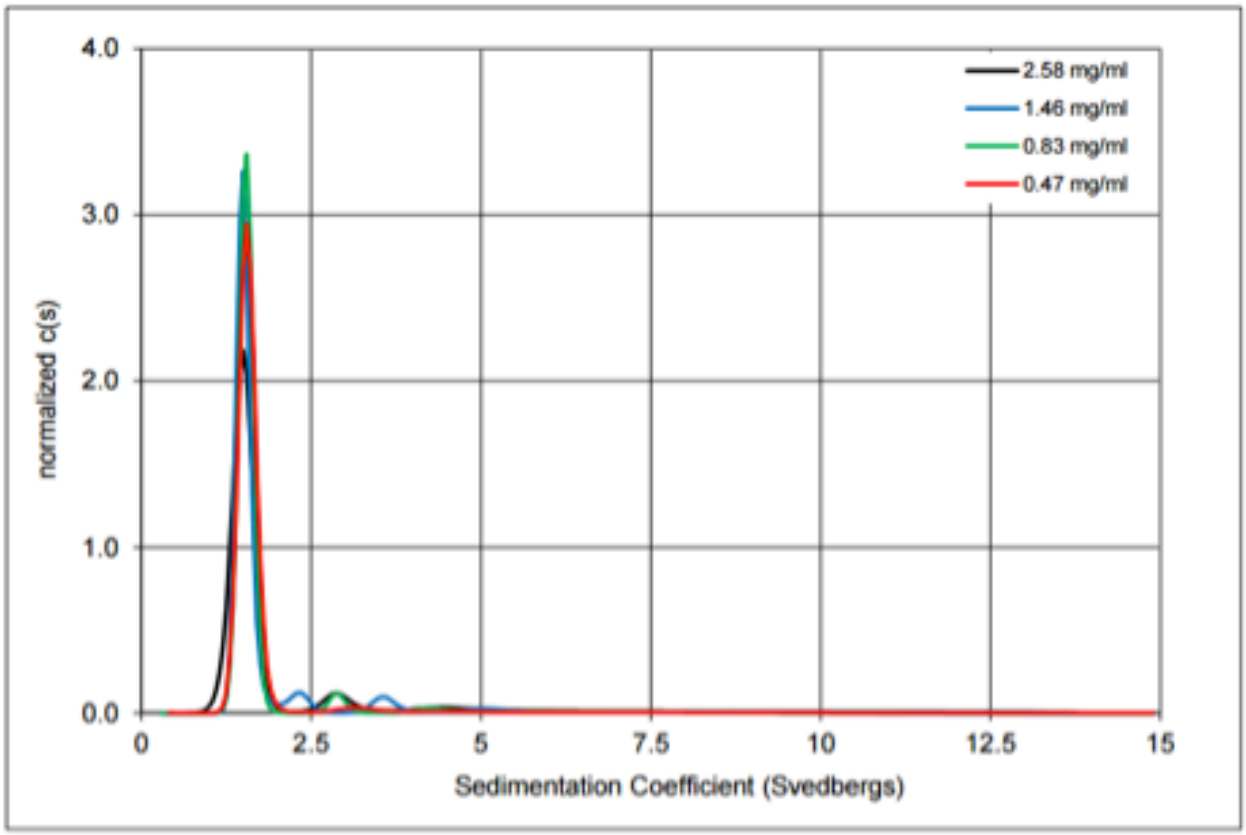

Figure S6. Related to Figure 3. Concentration dependence of ^{15}N-^{1}H backbone chemical shifts for NS1B CTD. The self-dissociation constant of NS1B-CTD was estimated by monitoring the chemical shift changes as a function of protein concentrations. The fitting of chemical shifts assumes a 1:1 protein-protein complex. The K_d was estimated using the larger of $^{1}H^{N}$ or ^{15}N chemical shift changes, as a function of protein concentration, as described elsewhere (Lee et al., 2010). (a) $^{1}H^{N}$ of K167, (b) $^{1}H^{N}$ of L240, (c) ^{15}N of G236, and (d) ^{15}N of F244.

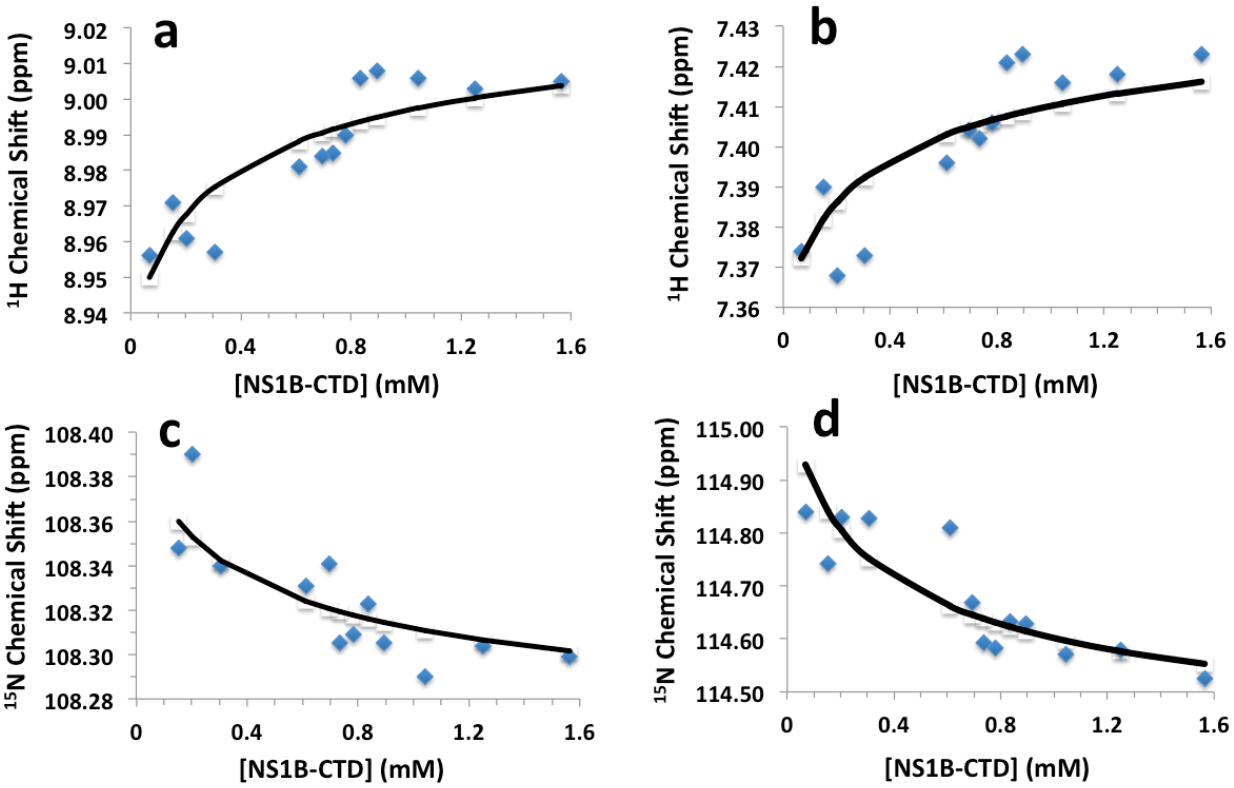

Figure S7. Related to Figures 2 and 7. The NS1A CTD from influenza A virus does not bind dsRNA. FP, in units of millipolarization (mP), resulting from binding of fluorescein-labeled 16-bp dsRNA [FAM-CCAUCCUCUACAGGCG (sense) and FAM-CGCCUGUAGAGGAUGG (antisense)] by NS1B CTD (black) and NS1A CTD (green). FAM-dsRNA was titrated with increasing protein concentration and the FP of FAM- RNA (20 nM) in the presence of different amounts of NS1B CTD and NS1A CTD (indicated on X-axis) was monitored. These measurements were performed in a buffer containing 25 mM NH_4OAc, pH 5.5, 225 mM NaCl, 5 mM $CaCl_2$, 1 mM EDTA, 1 mM TCEP, 25 mM Arg, and 0.02% NaN_3.

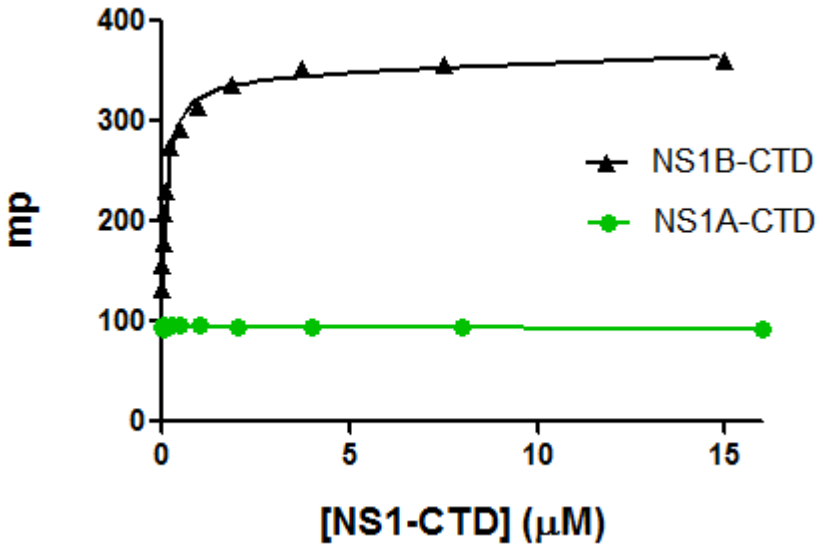

Figure S8. Related to Figures 1 and 3. NMR triple-resonance connectivity maps for backbone resonance assignments of wild-type and [R238A]-NS1B CTD. AutoAssign NMR connectivity maps (Moseley et al., 2001; Zimmerman et al., 1997) summarizing the triple-resonance NMR data used to determine the backbone resonance assignments of (a) wild-type NS1B CTD and (b) monomeric [R238A]-NS1B CTD mutant. Intraresidue (i) and sequential (s) triple-resonance NMR connectivities for the three-rung assignment strategy matching intraresidue and sequential C′, C^{α}, and C^{β} resonances are shown as horizontal red and yellow lines, respectively. Bar graphs of C^{α} and C^{β} Chemical Shift Index (CSI) (Wishart and Sykes, 1994) are shown in blue. The secondary structural elements in the final crystal structure of wt NS1B CTD (PDB id, 5DIL), shown above the sequence, correlate well with the CSI patterns observed by solution NMR. Protocols for this analysis are available on the NESG Wiki protocol site (http://www.nmr2.buffalo.edu/nesg.wiki/Main_Page).

Figure S8a. NMR triple-resonance connectivity map for wild-type NS1B CTD.

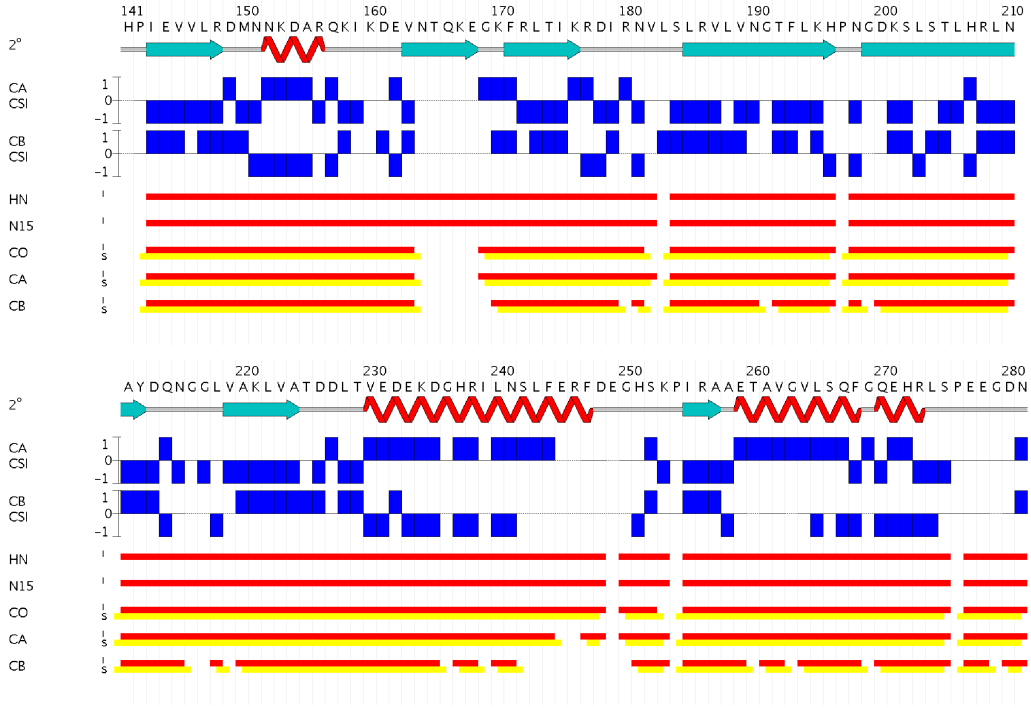

Figure S8b. NMR triple-resonance connectivity map for [R238A]-NS1B CTD.

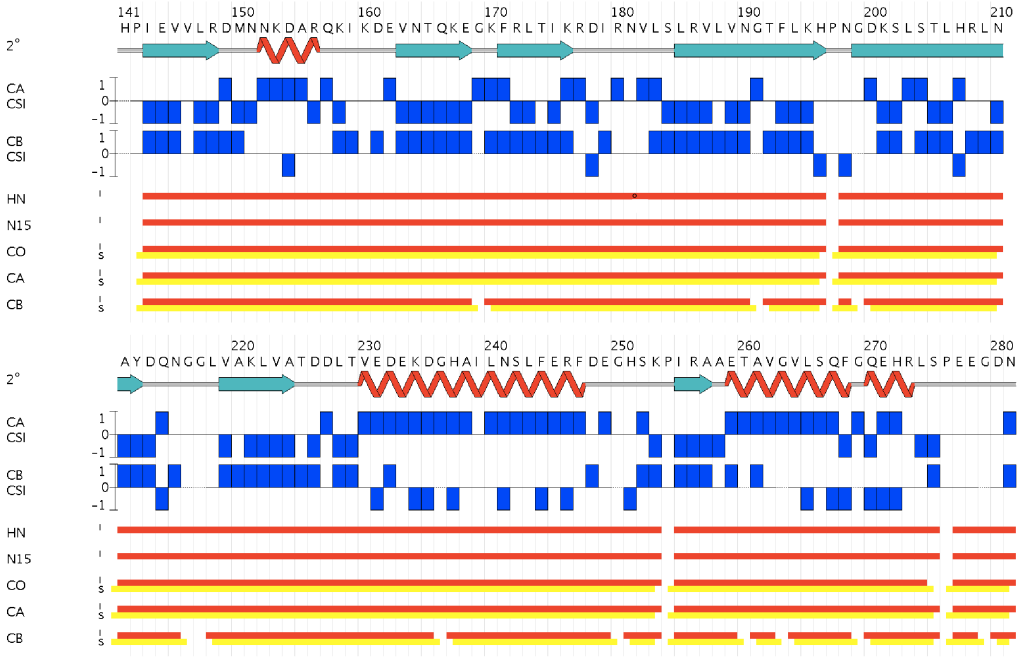

Supplemental Experimental Procedures

Cloning, expression, purification, and sample preparation. A DNA fragment encoding the effector domain of influenza B (B/lee/1940) NS1B-CTD (residues 141-281 of NS1B) was generated by PCR from the full-length gene and cloned into the modified pSUMO vector (LifeSensors), as described previously (Acton et al., 2011; Aramini et al., 2014; Aramini et al., 2011; Panavas et al., 2009) The NS1B-CTD construct was expressed as a N-terminal (6xHis)-tagged SUMO fusion protein in order to produce native NS1B-CTD following cleavage with SUMO protease. After sequence verification, the plasmid was transformed into *E. coli* strain BL21(DE3) cells containing the rare tRNA expression plasmid pMGK (Acton et al., 2011). Cells were first grown in LB media at 37 °C to an absorbance of 0.6 units at 600 nm, and then isopropyl-β-D-thiogalactoside (IPTG) was added to a final concentration of 1 mM to induce the expression of the SUMO fusion protein during 18 hours of incubation at 17 °C. For preparing selenomethionine-labeled NS1B-CTD, the cells were first grown in MJ9 minimal media at 37 °C to an absorbance of 0.6 at 600 nm, at which time selenomethionine, lysine, phenylalanine, threonine, isoleucine, leucine and were added (Doublie et al., 1996). IPTG induction was introduced after twenty minutes of incubation. The bacteria were harvested by centrifugation and resuspended in lysis buffer [50 mM Tris-HCl pH 7.5, 500 mM NaCl, 40 mM imidazole, and 1 mM Tris-(2-carboxyethyl)phosphine], followed by mild sonication. After high-speed centrifugation, the supernatant was applied to a 5 ml HisTrap™ affinity column (GE Healthcare), which was washed with the lysis buffer containing 5 M NaCl, and the protein was eluted using a buffer containing 50 mM Tris-HCl pH 7.5, 500 mM NaCl, 300 mM imidazole, and 1 mM Tris-(2 carboxyethyl) phosphine. Subsequently, the eluted protein sample, containing the SUMO fusion of NS1B CTD, was exchanged into cleavage buffer [50 mM Tris-HCl pH 8.0, 100 mM NaCl, and 10 mM dithiothreitol (DTT)] using a HiPrep 26/10 Desalting column (GE Healthcare). Alternatively, Econo-Pac® 10DG desalting columns (Bio-Rad) were used in preparing SUMO fusions of NS1B CTD variants for buffer exchange. The cleavage of the fusion protein was carried out by adding an aliquot (1:50–100 mass ratio) of yeast SUMO protease Ulp1 containing an N-terminal 6xHis tag (Ii et al., 2007), and the sample was then incubated at 25 °C for 18-24 hours. The degree of the cleavage was monitored by SDS-PAGE. To remove nucleic acid and SUMO, the mixture was applied to a 5 mL HiTrap™ heparin column (GE Healthcare), and the NS1B CTD was separated from nucleic acid and SUMO by gradient elution with 0 to 1 M or 2 M NaCl. Removal of nucleic acid was critical for providing samples suitable for NMR studies and for crystallization. Further purification was performed using size exclusion chromatography on a HighLoad 26/60 Superdex S75 column (GE Healthcare) equilibrated in 25 mM NH_4OAc (pH 5.5), 450 mM NaCl, 10 mM $CaCl_2$, 50 mM Arg, and 0.02% NaN_3. The purified NS1B-CTD was > 95% pure as determined by SDS/PAGE. The gel filtration elution peak containing NS1B-CTD was pooled and concentrated to 5 mg/mL and stored at −80 °C before being used for crystallization.

Production of isotope-enriched samples for NMR studies. U-^{13}C,^{15}N- and 5%-^{13}C,100%-^{15}N -labeled protein samples were produced using MJ9 medium (Jansson et al., 1996) containing $(^{15}NH_4)_2SO_4$ and D-[U-^{13}C]glucose as the sole nitrogen and carbon sources as described elsewhere (Acton et al., 2011). Triple-labeled [U-^{2}H,^{13}C,^{15}N]-NS1B CTD was expressed in MJ9 medium containing $(^{15}NH_4)_2SO_4$, [U-^{2}H,^{13}C]-D-glucose, and $^{2}H_2O$. Production of triple-labeled NS1B CTD containing protonated Ile-δ1, Leu-δ, and Val-γ methyl groups, [U-^{2}H,^{13}C,^{15}N; ^{1}H-Ile-δ1,Leu-δ,Val-γ]NS1B CTD was carried out using MJ9 medium containing $(^{15}NH_4)_2SO_4$, [U-^{2}H,^{13}C]-D-glucose, $^{2}H_2O$, [U-$^{13}C_4$, 3,3-$^{2}H_2$]α-ketobutyrate and [U-$^{13}C_5$, 3-^{2}H]α-ketoisovalerate (Goto et al., 1999). Protein samples were purified and characterized as described above. Isotope enrichment levels (>97%) were verified by MALDI-TOF mass spectrometry.

Crystallization and data collection High-throughput robotic crystallization screening of purified NS1B-CTD was carried out at the High Throughput (HTP) Crystallization Facility of the Hauptman-Woodward Medical Research Institute using the microbatch-under-oil method (Luft et al., 2003). Further

crystallization optimization was carried out using hanging drop evaporation method. The best crystals were obtained in 20% PEG 3350 with 0.2 M ammonium iodide, pH 5.6. Crystals were harvested with cryoloops (Hampton Research) and flash frozen in liquid N_2 before data collection using a home source Rigaku/MSC MicroMax-007 HF X-ray generator and an Rigaku *R-AXIS IV++* image plate detector, at the Center for Advanced Biotechnology and Medicine, Rutgers University. The space group of these crystals is *P*1. 360 frames were collected with an oscillation range of 1° and an exposure time of 120 seconds per frame. The X-ray diffraction images were indexed, integrated and scaled using *HKL2000* package (Otwinowski and Minor, 1997) and the data set was processed to 2.0 Å resolution.

Structure determination and refinement. Although there is only one methionine residue in this 141-281 construct, which could be problematic for phasing due to weak Se signals, the crystals were grown in a buffer containing iodide ions, which bound to the protein and served as heavy atoms for phasing. At the home X-ray source wavelength (1.54178 Å), the anomalous signal of iodide is very strong. The structure of NS1B-CTD was determined using the iodide SAD method with program AutoSol (Terwilliger et al., 2009) in Phenix (Adams et al., 2011) . With the phases and initial map from AutoSol, AutoBuild was used to build a model with more than 50% residues assigned. Structure refinement was carried out with program *PHENIX* (Adams et al., 2011). Manual model building and adjusting was done using COOT (Emsley and Cowtan, 2004), and the final model validated by the Protein Structure Validation Software Suite PSVS (Bhattacharya et al., 2007) and *MOLPROBITY* (Davis et al., 2007). Crystallographic statistics and final structure refinement and geometry statistics are summarized in Table 1.
NMR spectroscopy. NMR spectra of NS1B CTD and its mutants were carried out in buffered solutions containing 25 mM NH_4OAc (pH 5.5), 450 mM NaCl, 5 mM $CaCl_2$, 50 mM Arg, 0.02% NaN_3, 10% v/v ^2H_2O, using protein concentrations of 0.1 to 0.3 mM, excepted where noted otherwise. Spectra were acquired at 298 K on Bruker AVANCE 800 and 600 MHz spectrometers equipped with a 5-mm TXI and 1.7-mm TCI cryoprobes, respectively, and referenced to internal DSS (2,2-dimethyl-2-silapentane-5-sulfonic acid). All multi-dimensional NMR spectra were processed with NMRPipe (Delaglio et al., 1995) and visualized using the programs *Sparky* (Goddard and Kneller, 2000) or *CCPN-NMR* (Vranken et al., 2005).

Analytical gel filtration with multiangle static light scattering detection. AGF-MALS was carried out as previously described (Acton et al., 2005; Xiao et al., 2010). Briefly, an Agilent 1200 series HPLC system with an automated 96-well sample changer is used with a Shodex KW-802.5 HPLC size-exclusion column to separate the protein species in solution. A miniDAWN TREOS detector (Wyatt technologies) simultaneously measures light scattering at three different angles (45, 90, and 135 deg). Refractive index is also measured using an Optilab rEX Refractometer (Wyatt Technology). Together, the analysis of this data provides the shape-independent weight-average molecular mass of each species in the gel filtration effluent, and their relative distributions (Acton et al., 2005).

Analytical ultracentafugation. Sedimentation velocity and equilibrium ultracentrifugation analyses were carried out by the University of Connecticut Analytical Ultracentrafugation Facility, directed by Drs. J. L. Cole and J. W. Lary. A stock protein solution was supplied at an estimated protein concentration of 2 mg/ml, in a buffer containing 20 mM NH_4OAc, 450 mM NaCl, 5 mM $CaCl_2$, 50 mM Arginine, 0.02% NaN_3, at pH 5.5. A vial of the dialysate was also provided. The following physical constants were calculated from the sequence for the protein using the program Sednterp5: (Laue et al., 1992): MW_{seq} = 15.936 kDa, v_{20^o} = 0.7316 ml/g, A_{280} = 0.093 O.D.-mg^{-1}-ml^{-1}-cm^{-1}. The buffer density and viscosity were estimated to be 1.0218 g/ml and 0.01067 poise at 20 °C, respectively, using the Sednterp method (Laue et al., 1992). Sedimentation equilibrium experiments were performed at 20 °C using a Beckman XL-I instrument. The rotor was equilibrated under vacuum at 20 °C and after a period of ~1 hour at 20 °C the rotor was accelerated to 50,000 r.p.m. Interference scans were acquired at 60 second intervals for ~8 hours. Epon double sector centerpieces, equipped with sapphire windows, were loaded with 175 µL protein samples or buffer reference sample, respectively. Samples of solutions containing NS1B CTD

protein concentrations 13 to 100 mM were analyzed at 50,000 r.p.m. to determine the oligomeric state. Direct boundary modeling for individual data sets was done model based numerical solutions to the Lamm equation, and data were fit using the program Sedfit V13.0b (Shuck, 2000).

Sequence-specific resonance assignments and chemical shift perturbation studies. Near complete backbone ^{1}H, ^{13}C, and ^{15}N resonance assignments for wt and [R238A]-NS1B CTD (85-215) were determined using conventional triple resonance NMR methods (Supplementary Figure S8). Backbone assignments were made by a consensus analysis of output from both the PINE (Bahrami et al., 2009) and AutoAssign 2.4.0 (Moseley et al., 2001; Zimmerman et al., 1997) automated resonance assignment programs, using peak lists from TROSY-based (for wt NS1B CTD dimer) and standard (for [R238A]-NS1B CTD monomer) 2D [^{15}N-^{1}H]-HSQC and 3D HNCO, HN(CA)CO, HN(CO)CA, HNCA, CBCA(CO)NH or HN(CO)CACB, and HNCACB spectra acquired on [*U*-^{2}H,^{13}C,^{15}N; ^{1}H-Ile-δ1,Leu-δ,Val-γ]-NS1B CTD and [*U*-^{13}C,^{15}N]-[R238A]-NS1B CTD, respectively. Resonance assignments were validated using the Assignment Validation Suite (AVS) software package (Bhattacharya et al., 2007) and deposited in the BioMagResDB (BMRB accession numbers 25462 and 25463).

Supplemental References

Acton, T.B., Gunsalus, K.C., Xiao, R., Ma, L.C., Aramini, J., Baran, M.C., Chiang, Y.-W., Climent, T., Cooper, B., Denissova, N.G.*, et al.* (2005). Robotic cloning and protein production platform of the Northeast Structural Genomics Consortium. Meth Enzymol *394*, 210-243.

Acton, T.B., Xiao, R., Anderson, S., Aramini, J., Buchwald, W.A., Ciccosanti, C., Conover, K., Everett, J., Hamilton, K., Huang, Y.J.*, et al.* (2011). Preparation of protein samples for NMR structure, function, and small-molecule screening studies. Methods Enzymol *493*, 21-60.

Adams, P.D., Afonine, P.V., Bunkoczi, G., Chen, V.B., Echols, N., Headd, J.J., Hung, L.W., Jain, S., Kapral, G.J., Grosse Kunstleve, R.W.*, et al.* (2011). The Phenix software for automated determination of macromolecular structures. Methods *55*, 94-106.

Aramini, J.M., Hamilton, K., Ma, L.C., Swapna, G.V., Leonard, P.G., Ladbury, J.E., Krug, R.M., and Montelione, G.T. (2014). (19)F NMR reveals multiple conformations at the dimer interface of the nonstructural protein 1 effector domain from influenza A virus. Structure *22*, 515-525.

Aramini, J.M., Ma, L.C., Zhou, L., Schauder, C.M., Hamilton, K., Amer, B.R., Mack, T.R., Lee, H.W., Ciccosanti, C.T., Zhao, L.*, et al.* (2011). Dimer interface of the effector domain of non-structural protein 1 from influenza A virus: an interface with multiple functions. J Biol Chem *286*, 26050-26060.

Bahrami, A., Assadi, A.H., Markley, J.L., and Eghbalnia, H.R. (2009). Probabilistic interaction network of evidence algorithm and its application to complete labeling of peak lists from protein NMR spectroscopy. PLoS Comput Biol *5*, e1000307.

Bhattacharya, A., Tejero, R., and Montelione, G.T. (2007). Evaluating protein structures determined by structural genomics consortia. Proteins *66*, 778-795.

Davis, I.W., Leaver-Fay, A., Chen, V.B., Block, J.N., Kapral, G.J., Wang, X., Murray, L.W., Arendall, W.B., 3rd, Snoeyink, J., Richardson, J.S.*, et al.* (2007). MolProbity: all-atom contacts and structure validation for proteins and nucleic acids. Nucl Acids Res *35*, W375-383.

Delaglio, F., Grzesiek, S., Vuister, G.W., Zhu, G., Pfeifer, J., and Bax, A. (1995). NMRPipe: a multidimensional spectral processing system based on UNIX pipes. J Biomol NMR *6*, 277-293.

Doublie, S., Kapp, U., Aberg, A., Brown, K., Strub, K., and Cusack, S. (1996). Crystallization and preliminary X-ray analysis of the 9 kDa protein of the mouse signal recognition particle and the selenomethionyl-SRP9. FEBS Letts *384*, 219-221.

Emsley, P., and Cowtan, K. (2004). Coot: model-building tools for molecular graphics. Acta Cryst D *60*, 2126-2132.

Goddard, T.D., and Kneller, D.G. (2000). Sparky 3 (San Francisco, CA: University of California).

Goto, N.K., Gardner, K.H., Mueller, G.A., Willis, R.C., and Kay, L.E. (1999). A robust and cost-effective method for the production of Val, Leu, Ile (delta 1) methyl-protonated 15N-, 13C-, 2H-labeled proteins. J Biomol NMR *13*, 369-374.

Ii, T., Mullen, J.R., Slagle, C.E., and Brill, S.J. (2007). Stimulation of in vitro sumoylation by Slx5-Slx8: evidence for a functional interaction with the SUMO pathway. DNA repair *6*, 1679-1691.

Jansson, M., Li, Y.C., Jendeberg, L., Anderson, S., Montelione, B.T., and Nilsson, B. (1996). High-level production of uniformly 15N- and 13C-enriched fusion proteins in Escherichia coli. J Biomol NMR *7*, 131-141.

Laue, T.M., Shah, B., Ridgeway, T.M., and Pelletier, S.L. (1992). Computer-aided interpretation of sedimentation data for proteins. In Analytical Ultracentrifugation in Biochemistry and Polymer Science, S.E. Harding, A.J. Rowe, and J.C. Horton, eds. (Cambridge: Royal Society of Chemistry), pp. 90-125.

Lee, H.W., Wylie, G., Bansal, S., Wang, X., Barb, A.W., Macnaughtan, M.A., Ertekin, A., Montelione, G.T., and Prestegard, J.H. (2010). Three-dimensional structure of the weakly associated protein homodimer SeR13 using RDCs and paramagnetic surface mapping. Protein Sci *19*, 1673-1685.

Luft, J.R., Collins, R.J., Fehrman, N.A., Lauricella, A.M., Veatch, C.K., and DeTitta, G.T. (2003). A deliberate approach to screening for initial crystallization conditions of biological macromolecules. J Stuct Biol *142*, 170-179.

Moseley, H.N., Monleon, D., and Montelione, G.T. (2001). Automatic determination of protein backbone resonance assignments from triple resonance nuclear magnetic resonance data. Methods Enzymol *339*, 91-108.

Otwinowski, Z., and Minor, W. (1997). Processing of X-ray diffraction data collected in oscillation mode. . Methods Enzymol *276*, 307-326.

Panavas, T., Sanders, C., and Butt, T.R. (2009). SUMO fusion technology for enhanced protein production in prokaryotic and eukaryotic expression systems. Methods Mol Biol *497*, 303-317.

Shuck, P. (2000). Size distribution analysis of macromolecules by sedimentation velocity ultracentrifugation and Lamm equation modeling. Biophysical Journal *78*, 1606-1619.

Terwilliger, T.C., Adams, P.D., Read, R.J., McCoy, A.J., Moriarty, N.W., Grosse-Kunstleve, R.W., Afonine, P.V., Zwart, P.H., and Hung, L.W. (2009). Decision-making in structure solution using Bayesian estimates of map quality: the PHENIX AutoSol wizard. Acta Cryst Section D, Biological crystallography *65*, 582-601.

Vranken, W.F., Boucher, W., Stevens, T.J., Fogh, R.H., Pajon, A., Llinas, M., Ulrich, E.L., Markley, J.L., Ionides, J., and Laue, E.D. (2005). The CCPN data model for NMR spectroscopy: development of a software pipeline. Proteins *59*, 687-696.

Wishart, D.S., and Sykes, B.D. (1994). The C-13 Chemical-Shift Index - a simple method for the identification of protein secondary structure using C-13 chemical-shift data. J Biomol NMR *4*, 171-180.

Xiao, R., Anderson, S., Aramini, J., Belote, R., Buchwald, W.A., Ciccosanti, C., Conover, K., Everett, J.K., Hamilton, K., Huang, Y.J.*, et al.* (2010). The high-throughput protein sample production platform of the Northeast Structural Genomics Consortium. J Struct Biol *172*, 21-33.

Zimmerman, D.E., Kulikowski, C.A., Huang, Y., Feng, W., Tashiro, M., Shimotakahara, S., Chien, C., Powers, R., and Montelione, G.T. (1997). Automated analysis of protein NMR assignments using methods from artificial intelligence. J Mol Biol *269*, 592-610.